1 HT-SIP: A semi-automated Stable Isotope Probing pipeline identifies interactions in the

2 hyphosphere of arbuscular mycorrhizal fungi

- 3
- 4 Erin E. Nuccio¹* (nuccio1@llnl.gov), Steven J. Blazewicz¹ (blazewicz1@llnl.gov), Marissa Lafler¹
- 5 (<u>mlafler@gmail.com</u>), Ashley N. Campbell¹ (<u>a.campbell910@gmail.com</u>), Anne Kakouridis^{2,3}
- 6 (annekakouridis@lbl.gov), Jeffrey A. Kimbrel¹ (kimbrel1@llnl.gov), Jessica Wollard¹
- 7 (wollard1@llnl.gov), Dariia Vyshenska⁴ (dariiavyshenska@lbl.gov), Robert Riley⁴ (rwriley@lbl.gov),
- 8 Andy Tomatsu⁴ (atomatsu@lbl.gov), Rachel Hestrin^{1,5} (rhestrin@umass.edu), Rex R. Malmstrom⁴
- 9 (<u>rrmalmstrom@lbl.gov</u>), Mary Firestone³ (<u>mkfstone@berkeley.edu</u>), Jennifer Pett-Ridge^{1,6}*
- 10 (pettridge2@llnl.gov)
- 11
- ¹Lawrence Livermore National Laboratory, Physical and Life Science Directorate, Livermore, CA, USA
- 13 ²Lawrence Berkeley National Laboratory, Biosciences Division, Berkeley, CA, USA
- ³University of California, Berkeley, Department of Environmental Science Policy and Management,
- 15 Berkeley, CA USA
- ⁴DOE Joint Genome Institute, Berkeley, CA, USA
- ⁵University of Massachusetts, Stockbridge School of Agriculture, Amherst, MA, USA
- ⁶University of California Merced, Life & Environmental Sciences Department, Merced, CA 95343 USA
- 19
- 20 *Co-Corresponding authors
- 21

22

23 ABSTRACT

24 Background: Linking the identity of wild microbes with their ecophysiological traits and environmental 25 functions is a key ambition for microbial ecologists. Of many techniques that strive to meet this goal, 26 Stable Isotope Probing—SIP—remains the most comprehensive for studying whole microbial 27 communities in situ. In DNA-SIP, active microorganisms that take up an isotopically heavy substrate 28 build heavier DNA, which can be partitioned by density into multiple fractions and sequenced. However, 29 SIP is relatively low throughput and requires significant hands-on labor. We designed and tested a semi-30 automated DNA-SIP pipeline to support well-replicated, temporally-resolved amplicon or metagenomics 31 experiments that enable studies of dynamic microbial communities over space and time. To test this 32 pipeline, we assembled SIP-metagenome assembled genomes (MAGs) from the hyphosphere zone 33 surrounding arbuscular mycorrhizal fungi (AMF), in combination with a ¹³CO₂ plant labelling study. 34 Results: Our semi-automated pipeline for DNA fractionation, cleanup, and nucleic acid quantification of 35 SIP density gradients requires six times less hands-on labor compared to manual SIP and allows 16 36 samples to be processed simultaneously. Automated density fractionation increased the reproducibility of 37 SIP gradients and reduced variation compared to manual fractionation, and we show adding a non-ionic 38 detergent to the gradient buffer improved SIP DNA recovery. We then tested this pipeline on samples 39 from a highly-constrained soil microhabitat with significant ecological importance, the AMF fungal 40 hyphosphere. Processing via our quantitative SIP pipeline confirmed the AMF Rhizophagus intraradices 41 and its associated microbiome were highly ¹³C enriched, even though the soils' overall enrichment was 42 only 1.8 atom% ¹³C. We assembled 212 ¹³C-enriched hyphosphere MAGs, and the hyphosphere taxa that 43 assimilated the most AMF-derived ¹³C (range 10-33 atom%) were from the phlya Myxococcota, 44 Fibrobacterota, Verrucomicrobiota, and the ammonia oxidizing archaeon genus Nitrososphaeara.

46	Conclusions: Our semi-automated SIP approach decreases operator time and errors and improves
47	reproducibility by targeting the most labor-intensive steps of SIP-fraction collection and cleanup. Here,
48	we illustrate this approach in a unique and understudied soil microhabitat-generating MAGs of active
49	microbes living in the AMF hyphosphere (without plant roots). Their phylogenetic composition and gene
50	content suggest predation, decomposition, and ammonia oxidation may be key processes in hyphosphere
51	nutrient cycling.
52	
53	KEYWORDS
54	Stable Isotope Probing, metagenomics, microbial community, Arbuscular Mycorrhizal Fungi, SIP, AMF,
55	soil, bacteria, archaea, ammonia oxidation
56	
57	
58	

59 BACKGROUND

60	Stable isotope probing 'SIP' approaches, where active microbes are identified via incorporation of stable
61	isotopes (¹³ C, ¹⁵ N, ¹⁸ O) into their biomarkers, cells, DNA or RNA, are among the most powerful methods
62	in microbial ecology since they can identify the most relevant active microbes and their specific
63	ecophysiology traits in natural, 'wild' settings [1-7]. Broadly speaking, SIP refers to any technique where
64	microorganisms that have consumed substrates enriched in rare stable isotopes (e.g. ¹³ C, ¹⁵ N, ¹⁸ O) are
65	identified based on the resulting isotopic enrichment of their nucleic acids, proteins, and metabolites
66	(reviewed in [5, 8]). However, DNA-SIP-where isotopically enriched DNA is separated from
67	unenriched nucleic acids via isopycnic separation in cesium chloride—is the most commonly used SIP
68	approach, typically in conjunction with 16S rRNA gene or shotgun metagenome analysis. A cornerstone
69	of many seminal studies of microbial biogeochemical cycling, DNA-SIP has been used to identify
70	populations involved in decomposer food webs [9], consume plant root exudates [10, 11], degrade
71	pollutants [12] and C1 compounds [13], oxidize ammonia [14], fix N2 [15, 16], or to characterize
72	population growth, survival and mortality in mixed communities [17, 18].
73	Quantitative stable isotope probing (qSIP) and techniques such as 'high resolution' SIP (HR-SIP)
74	[19] are expansions of the original SIP concept that combine density gradient ultracentrifugation with
75	mathematical models designed to improve the quantification (sensitivity and specificity) of isotope
76	enrichment [6, 20]. When used with a ¹⁸ O-enriched 'heavy water' addition, qSIP enables calculation of
77	growth and mortality rates of individual taxa, since cells and viruses incorporate oxygen from water
78	during nucleic acid synthesis, quantitatively reflecting cell division (DNA synthesis) and metabolism
79	(RNA synthesis) [21-23]. Recent qSIP studies have used the method to illustrate how wild microbial
80	communities are shaped by evolutionary history [24, 25], soil temperature and warming [26, 27],
81	amendments of water and nutrients [18, 28] and trophic relationships amongst bacterial predators and
82	their prey [29].

83 While the majority of SIP and qSIP studies have focused on 16S rRNA gene profiles, targeting 84 active populations with shotgun sequencing (metagenomes and metatranscriptomes) provides greater 85 opportunity for inference of genomic potential and whole genome-scale data analysis [30-32], define 86 microbial guilds [33], and provide insights into cross-kingdom interactions (including virus-host 87 matching) [23, 34]. But SIP-metagenomics is a daunting prospect for many research groups, as multiple 88 metagenome datasets are generated from each initial microbiome DNA sample, creating financial and 89 computational limitations that constrain experimental scope. Sieradzki et al. (2020) [35] explain the 90 relationships between sample replication, enrichment and the precision achievable with a given number of 91 SIP density fractions (and suggest 9 fractions is typically ideal). Additionally, processing SIP density 92 gradients is a relatively low throughput process and requires significant hands-on labor, making it onerous 93 to conduct the well-replicated, temporally resolved experiments needed to study dynamic microbial 94 community activities over space and time. Historically, SIP studies have used few replicates due to the 95 laborious nature of the technique. To address this short-coming, we have designed a high-throughput SIP 96 (HT-SIP) pipeline for processing SIP density gradients, which automates fractionation, partially 97 automates fraction cleanup, and automates the preparation of samples for nucleic acid quantification. We 98 have now tested replicates of this pipeline at both LLNL and the JGI for over two years, running 1000s of 99 samples.

100 To validate and demonstrate the utility of our HT-SIP pipeline on an important yet challenging 101 sample set, we targeted the 'hyphosphere' soil microhabitat using ¹³C labeling—the area under direct 102 influence of arbuscular mycorrhizal fungal (AMF) hyphae. Arbuscular mycorrhizal fungi (members of the 103 Glomeromycota) form obligate symbiotic associations with 80% of all land plants [36], and in exchange 104 for plant carbon (C), supply their host with essential nutrients such as N and P [37, 38] and water [39]. 105 Intriguingly, AMF are capable of stimulating decomposition of soil organic matter (SOM) and dead plant 106 material [40-42], but do not have the enzymatic repertoire to decompose SOM themselves. As such, the 107 importance of interactions with the soil microbiome is potentially critical [43], and previous research

108 suggests that AMF modify their surrounding soil litter-decomposing microbial community in order to 109 acquire nitrogen derived from SOM, and transport it to the host plant [38, 44]. However, these 110 interactions occur at such a small spatial scale (hyphae are ca. $1.5 - 18 \mu m$ in diameter [45]) that they are 111 extremely difficult to measure and monitor. Using SIP, in conjunction with ¹³CO₂ labeling of a plant host 112 inoculated with AMF, we tracked plant-fixed carbon through AMF hyphae and into the surrounding 113 hyphosphere microbiome. 114 To generate SIP-metagenomes from the AMF-hyphosphere, we ¹³CO₂ labeled the wild annual 115 grass, Avena barbata, inoculated with the AMF Rhizophagus intraradices in sterile sand. The 116 microcosms contained a separate hyphal chamber with live soil that only AMF hyphae could access, from which hyphal aggregates were collected and extracted for ¹³C-hyphosphere SIP processing. We used our 117 118 semi-automated pipeline to process samples from this microhabitat, and produced high quality libraries 119 and MAGs even while using an unusually low starting DNA input for SIP separations (350 ng DNA). Our 120 work demonstrates that automation not only saves operator time and improves reproducibility of SIP 121 processing, but is also suitable for analysis of low DNA quantities and downstream amplicon and 122 metagenomics analysis. The ¹³C-hyphosphere MAGs assembled in this study are a key advance for 123 dissecting trophic interactions in the AMF hyphosphere.

125 METHODS

126 Density Gradient Separations

127 HT-SIP validation experiments were conducted using 1-5 µg DNA for SIP density gradient separations

- 128 (below, amounts and DNA sources are specified per experiment). To separate DNA based on isotopic
- 129 enrichment, DNA was added to 150 µL 1xTE buffer mixed with 1.00 mL gradient buffer, and 4.60 mL
- 130 CsCl stock (1.885 g mL⁻¹) with a final density of 1.725-1.730 g mL⁻¹. Samples were loaded into
- 131 ultracentrifuge tubes (5.1 mL, Quick-Seal Round-Top Polypropylene Tube, Beckman Coulter) and spun
- 132 at 20°C for 108 hours at 176,284 RCF_{avg} (equivalent to 176,284 x g) in a Beckman Coulter Optima XE-90
- 133 ultracentrifuge using a VTi65.2 rotor, following a previously described protocol [17, 35] to create density
- 134 gradients.
- 135

136 High-Throughput SIP (HT-SIP) Pipeline

137 To automate the labor-intensive steps of SIP—density gradient fractionation, cleanup, and

138 quantification—we combined a series of robotic instruments. Following cesium chloride (CsCl) density

139 gradient separation in an ultracentrifuge, we automated fractionation by connecting an Agilent

140 Technologies 1260 Isocratic Pump and 1260 Fraction Collector to a Beckman Coulter Fraction Recovery

141 System (see Supplemental Figure S1 for schematic and parts list). In this system, each sample is separated

142 into 22 fractions (~236 µL each). CsCl is displaced in the ultracentrifuge tube by pumping sterile water at

143 0.25 mL min⁻¹ through a 25G needle inserted into the top of the ultracentrifuge tube, and the sample

144 fraction exits via a side port needle inserted into the bottom of the tube. We maintain pressure between 1-

145 1.8 bar; pressures above this indicate the system is clogged. The gradient medium fractions are dispensed

146 into 96-well deep well plates (2 ml square well plates with v-bottoms, Stellar Scientific) by the Agilent

- 147 Fraction Collector. Four SIP tubes are fractionated into a single deep-well plate (88 wells) and the final
- 148 row is left empty for PicoGreen quantification standards. At the beginning of the day and after every four
- 149 gradients, we clean the fractionation tubing with water using a "wash spacer" to bypass the fraction
- 150 recovery system (see Supplemental Figure S1). The density of each fraction is measured manually using a

151 Reichart AR200 digital refractometer fitted with a prism covering to facilitate measurement from 5 μ L, as 152 previously described [46].

153 DNA in each density fraction is then purified (desalted) and concentrated using a Hamilton 154 Microlab STAR liquid handling robot, which we have programmed to automate PEG precipitations using 155 a previously published protocol [47], with modifications for 96-well plates. We configured our robot deck 156 to process four plates; this allows a maximum of 16 SIP samples to be processed simultaneously (4 157 samples per plate). Following fractionation, the robot adds 2 volumes of 30% PEG 6000 (in 1.6 M NaCl) 158 and 35ul of 1:5 diluted Glycoblue (Invitrogen, Thermo Fisher) to each well. Plates are then manually 159 sealed and mixed thoroughly by vortexing and manual shaking, pulsed down briefly, and incubated at 160 room temperature in the dark overnight. To precipitate the DNA, we spin the four plates at 4198 RCF for 161 5 hours at 20°C in an Eppendorf 5920R centrifuge using a S-4xUniversal-Large rotor. The plates are then 162 placed back in the Hamilton robot, which removes the PEG by pipetting and rinses the pellets using 950ul 163 70% ethanol. Plates are manually sealed, gently mixed by vortexing, and centrifuged at 4198 RCF for 1.5 164 hours at 20°C to stabilize the DNA pellets. We aspirate the ethanol with the robot, and then manually 165 place the plates upside down on a paper towel to drain remaining ethanol. The plates are then returned to 166 the robot to dry for 15 minutes, whereafter the robot automatically resuspends the DNA pellets in 40 μ L 167 of 1x Tris-EDTA (pH 7.5); 10 mM Tris-HCl may be used for applications sensitive to EDTA. Finally, 168 plates are manually sealed and stored at -20°C. 169 Finally, DNA concentration of each fraction is quantified with a PicoGreen fluorescence assay 170 (Invitrogen, Thermo Fisher). Picogreen quantification plates are prepared in triplicate on a Hamilton 171 Microlab STAR robot, where each plate contains a row for the standard curve. Samples are mixed with

172 the PicoGreen reagent in a 96-well intermediate mixing plate, and then distributed into three 96-well PCR

173 plates for fluorescence analysis. Plate fluorescence is measured in a CFX Connect Real-Time PCR

174 Detection System (Bio-Rad), and the fluorescence values for the three technical replicate plates are

175 averaged to determine DNA concentration.

177 Validation of HT-SIP using Manual SIP

178 To validate the automated steps of our HT-SIP pipeline, we compared fractionation and PEG 179 precipitations using both manual and automated methods. Automated fractionation was performed as 180 described above, and manual fractionation was conducted with a Beckman Coulter fraction recovery 181 system as previously described [17]. Samples were fractionated into approximately 22 fractions, although 182 the number of fractions recovered by manual SIP typically varies despite identical run conditions. 183 To compare automated verses manual PEG precipitations, 4 ug soil DNA (extracted from a 184 sample collected at the Hopland Research and Extension Center in Hopland, CA 38°59'35"N, 123°4'3"W) 185 was added per density gradient. For manual samples, following manual fractionation, PEG precipitations 186 were conducted in microcentrifuge tubes as previously described [47] using published centrifuge speeds 187 and times, which we note are faster than those used for our HT-SIP plate-based method. 188 189 Increasing DNA-SIP recovery using non-ionic detergents 190 Absorption of DNA to polypropylene tubes can lead to substantial sample loss, especially for DNA in 191 high ionic strength solutions [48], but this concern can be mitigated by adding non-ionic detergents [48]. 192 Since the ultracentrifuge tubes used in DNA-SIP protocols are made of polypropylene and CsCl is a high 193 ionic strength solution, we tested whether adding the non-ionic detergents Tween-20 and Triton-X to 194 density gradient buffer improved DNA recovery. To identify the optimal concentration of detergent for 195 DNA-SIP recovery, we tested additions in the range of 0.0001 - 1% for Tween-20 and 0.0001 - 0.1% for 196 Triton-X and compared DNA recovery versus the standard density gradient formulation. 1 ug of E. coli 197 genomic DNA (Thermo Scientific) was added to density gradients and processed using the HT-SIP 198 pipeline (n=3 gradients per condition). After identifying that adding 0.0001% Tween-20 had the highest 199 percent DNA recovery, we assessed 0.0001% Tween-20 additions to a larger set of soil DNA samples 200 (101 SIP tubes total) using our HT-SIP pipeline. We added 4 µg of soil DNA (from Hopland, CA soil) to 201 these gradients.

203 Validation of HT-SIP Pipeline: Hyphosphere ¹³CO₂ Labeling and Harvest

AMF hyphosphere soil was ¹³C-labeled in ¹³CO₂ plant growth chambers; details on the microcosm design and growth conditions are documented in [39]. Briefly, *Avena barbata* seedlings were planted in the 'plant compartment' of two-compartment microcosms and grown for 10 weeks. The plant compartment was separated from the 'no-plant compartment' by a 3.2 mm air gap to prevent root exudates or dissolved organic C from travelling via mass flow between compartments. Both sides of the air gap had nylon mesh that either allowed hyphae but excluded roots (18 μ m mesh), or that excluded both hyphae and roots (0.45 μ m mesh).

- 211 In the plant compartment, a sterile sand mix (1:1 volumes of sand and clay, plus 78 mg of
- autoclaved bonemeal) was inoculated with 26 g of whole inoculum of *Rhizophagus intraradices*

213 (accession number AZ243, International Culture Collection of (Vesicular) Arbuscular Mycorrhizal Fungi

214 (INVAM), West Virginia University, Morgantown, WV). The no-plant compartment contained a mixture

of 1:1 volumes of live soil (from Hopland CA) and sand plus 78 mg of autoclaved bone meal.

216 The microcosms were incubated in growth chambers in the Environmental Plant Isotope Chamber

217 (EPIC) facility, located in the Oxford Tract Greenhouse at UC Berkeley, in temperature-controlled

218 growth chambers with a multiplexed ¹³CO₂ delivery system monitored by IRGA and Picarro CO₂

analyzers. For this study, three microcosms with 18 µm mesh (¹³C AMF permitted in the no-plant

220 compartment, termed '¹³C-hyphosphere') and three microcosms with 0.45 μm mesh (¹³C AMF excluded

from the no-plant compartment, termed ¹³C no-AMF control', for IRMS analysis only) were

222 continuously ¹³CO₂-labeled for 6 weeks during weeks 5-10. Six additional microcosms remained in a

223 natural abundance CO_2 atmosphere for the full ten weeks; of these, the three ¹²C microcosms with 18 μ m

224 mesh (¹²C AMF permitted in the no-plant compartment, termed '¹²C-hyphosphere') served as the ¹²C-

225 hyphosphere SIP controls, and three ¹²C microcosms with 0.45 µm mesh (¹²C AMF excluded from the no-

226 plant compartment) were for IRMS analysis only. AMF-specific Sanger sequencing of the plant

227 compartment (roots, sand) as well as the air-gap indicated the planted compartment only contained the

initial mycorrhizal inoculum [39].

229	At the beginning of week 11, all microcosms were destructively sampled. Soil was placed in				
230	Whirl-Pak bags, flash frozen in liquid nitrogen, and stored at -80°C. To collect hyphosphere microbia				
231	communities, visible hyphal aggregates with hyphosphere soil attached were collected from the no-plan				
232	compartments using tweezers under a dissecting microscope for +AMF microcosms. For no-AMF				
233	controls, the soil mix was sampled the same way, except no hyphae were visible. During the microcosm				
234	harvest, plant shoots, roots, and soil from the planted and unplanted chambers were placed in paper				
235	envelopes and then dried 60°C for 72 hours for ¹³ C IRMS analysis. These samples were finely ground,				
236	weighed, and analyzed for total C and ¹³ C abundance by dry combustion on a PDZ Europa ANCA-GSL				
237	elemental analyzer interfaced to a PDZ Europa 20-20 isotope ratio mass spectrometer (Sercon Ltd.,				
238	Cheshire, UK). Stated precision by the manufacturer for ${}^{13}C$ is 0.1 per mil.				
239					
240	Hyphosphere HT-SIP Density Gradient Separations				
241	DNA was extracted from 250 mg of hyphal aggregates using the DNeasy PowerSoil kit (Qiagen). We				
242	added 350 ng of ¹³ C- and ¹² C-hyphosphere hyphosphere DNA ($n = 3$ each) to density gradients and				
243	ultracentrifuged as described above, and then fractionated, precipitated, and quantified using the HT-SIP				
244	pipeline. DNA pellets were resuspended in 10mM Tris-HCl (pH 7.5) because the low DNA mass in each				
245	fraction required us to use a large fraction volume during sequence library creation and would have				
246	resulted in higher than recommended EDTA concentrations (< 0.1 mM EDTA final concentration).				
247					
A 40					

248 *Metagenomic Sequencing Library Preparation and Sequencing*

249 Since the overall soil ¹³C-enrichment was relatively low in these samples, we sequenced metagenomes

250 from 14 fractions per sample to increase the chance of detecting taxa with significant ¹³C-enrichment;

251 Sieradzki et al. [35] have shown that sensitivity is correlated with isotopic enrichment. Fractions with low

concentrations of DNA at the beginning (fractions 3-6) and end of the gradient (fractions 19-21) were

- 253 combined and concentrated prior to sequencing using an Amicon Ultra-0.5 30KDa filter (Millipore
- 254 Sigma) [49]; fractions 7-18 were sequenced without concentration. Whole genome metagenomic libraries

255 were prepared at LLNL using the Illumina DNA Flex library kit (now called Illumina DNA Prep, 256 Illumina Inc., Santa Clara, CA) using 1 ng of sample DNA and 12 cycles of amplification. The libraries 257 were dual indexed with Illumina Nextera DNA CD indexes following the manufacturer's recommended 258 protocol and quantified using a Qubit broad range dsDNA assay (Thermo Fisher Scientific, Waltham, 259 MA). Library insert sizes were determined via Agilent Tapestation with the D5000 High Sensitivity assay 260 (Agilent Technologies, Santa Clara, CA). Equimolar amounts of each library were pooled together. The 261 pooled libraries' sizes and concentrations were verified using the D5000 High Sensitivity assay (Agilent 262 Technologies, Santa Clara, CA). 263 The library was diluted and denatured as described [50] to a final concentration of 375 pM (2% 264 phiX and 98% library). The library pools were sequenced with NextSeq 1000/2000 P2 or P3 reagents 265 (Illumina Inc., Santa Clara, CA) as paired end 2 X 150 cycles on an Illumina NextSeq2000 Sequencer at 266 Lawrence Livermore National Laboratory. In total, 2.6x10⁹ read pairs passed quality filtering, with a mean of 3.1×10^7 read pairs per sample/fraction and a range of 3.0×10^6 to 1.1×10^8 read pairs. 267

268

269 *Metagenome Assembly*

270 Our prior research indicates that coassemblies of all SIP gradient fractions from biological replicates yield 271 the best metagenome-assembled genomes (MAGs) [31, 51]. Metagenomic sequences were loaded into 272 IMG v5.1.1. We created individual assemblies using metaspades [52] and a single co-assembly including 273 all fractions using MetaHipMer v2 [51]. MetaHipMer produced more contigs (Supplemental Table S2), 274 so we proceeded with this assembly. Sequences were mapped to the assembly using bbmap [53], binned 275 with Metabat v2.12.1, and then bins were refined with metaWRAP v1.2.1 [54]. MAG quality was 276 determined by CheckM v1.1.3 [55], taxonomy determined by GTDB-tk v1.50 with version r202 of the 277 GTDB taxonomy database [56] and final metrics are reported using Minimum Information about a 278 Metagenome Amplified Genome (MIMAG) standards [57]. MAG abundances were determined using 279 bbsplit [53]. The sequenced genome of *Rhizophagus irregularis* DAOM 197198 was included in the 280 bbsplit reference library to map AMF sequences (RefSeq assembly accession: GCF 000439145.1) [58].

281	The genomic capacities of high- and medium-quality MAGs of highly ¹³ C enriched hyphosphere
282	taxa were determined by annotating into functional categories with Patric subsystems [59] and KEGG
283	orthologs from KofamKOALA [60]. Carbohydrate active enzyme (CAZyme) gene homologs were
284	determined using dbCAN HMM analysis [61]. Protease homologs were determined using blastp against
285	the MEROPS v.12.1 database [62]; an initial screen was performed using the "merops_scan.lib" database,
286	and positive hits were then compared to the larger "pepunit.lib" database, which is a non-redundant
287	library of all peptidase units and inhibitor units in MEROPS.

288

289 *Quantitative SIP Analysis*

290 We applied quantitative SIP (qSIP) calculations to estimate the atom percent excess (APE) 13 C

291 enrichment for each taxon following procedures detailed in Hungate et al. [20] with adjustments for

292 metagenome-assembled genomes instead of 16S rRNA genes [31, 34]. qSIP uses the number of reads per

fraction across the SIP gradient to estimate the APE of each taxon within the enriched sample compared

to the natural abundance control. To estimate the amount of taxon-specific DNA per fraction, we

295 calculated the proportion of the library attributable to the MAG and multiplied by the DNA content per

fraction ([MAG_counts / total_library_counts] * ng_fraction_DNA). Since our reference database of

297 MAGs is incomplete, and does not include genomes for eukaryotes and fungi other than the AMF *R*.

298 *intraradices*, we normalized MAG counts to total sequencing library counts because this includes the

299 portion of the library with no sequenced representatives. After the MAG sequence counts were converted

300 into estimates of DNA mass (ng), weighted average densities (WAD) for each MAG were calculated for

301 each gradient. The differences in WAD between the ¹³C and ¹²C gradients were used to estimate the atom

302 percent excess for each MAG [20]. All MAGs were present in all three replicates. To be considered ¹³C-

303 enriched, the 90% lower confidence interval of a MAG's median APE- 13 C needed to be >0% APE- 13 C.

304 **RESULTS**

305 Reproducibility of automated fractionation

Automated fractionation increased the reproducibility of fractionation; the buoyant densities of automated samples had a more consistent linear fit across gradients ($r^2 = 0.984$, n = 24 gradients) compared to manually fractionated gradients ($r^2 = 0.908$, n = 22 gradients) (**Figure 1**). With manual fractionation, the sample to sample variability of fraction density increased in fractions collected later in the process (less dense) and resulted in a more variable number of fractions even though identical fractionation conditions were used (range = 15 - 27 fractions); in contrast, automated fractionation consistently resulted in 22 fractions.

313

314 Effect of non-ionic detergents on automated DNA recovery

315 Post-fractionation DNA recovery is a key concern for DNA-SIP studies, especially for samples where 316 total DNA volume is limited. In our initial testing of >1000 environmental DNA samples (at LLNL and 317 JGI), we noticed DNA percent recovery tended to improve when larger masses of DNA were added to the 318 density gradient (3-5 µg) and hypothesized that DNA was being lost by an adsorption mechanism. We 319 therefore tested how adding the non-ionic detergents Tween-20 and Triton-X affected DNA recovery in 320 density gradients, which can mitigate potential DNA loss by adsorption to polypropylene tube walls [48]. 321 Adding Tween-20 at final concentrations $\leq 0.01\%$ reliably increased the recovery of 1 µg pure culture E. 322 *coli* DNA, and Tween-20 at 0.0001% yielded the highest overall DNA recovery $(84 \pm 5\%)$ compared to a 323 no-detergent control ($64 \pm 5\%$ recovery) (Supplemental Table S1). Triton-X only improved DNA 324 recovery at a final concentration of 0.0001% (74 ± 3%). 325 Using soil DNA in the absence of Tween-20, we had higher DNA recovery with manual 326 processing (measured after the precipitation step) relative to the automated protocol (Figure 2a). When 327 0.0001% Tween-20 was included in the density gradient buffer, soil DNA recovery with the automated

328 protocol was comparable to the manual approach (Figure 2). For the automated protocol, adding Tween-

329 20 significantly increased soil DNA yields by a factor of 1.8 from 35 ± 4% to 64 ± 3% (mean ± 95% CI; p
330 < 0.01 for one-tailed t-test) (Figure 2b).

331

332 SIP automation time savings

333 In HT-SIP, automating multiple steps in sample SIP processing substantially increased the overall speed 334 of the procedure and decreased the amount of manual or "hands-on" labor required. Using automation 335 during fraction collection, sample cleanup, and DNA quantification, it is manageable to process 16 336 samples in parallel (this batch number is constrained by the typical number of spaces available in an 337 ultracentrifuge rotor). Overall, HT-SIP requires half as much technician time to fully process 16 samples 338 (42 h versus 20 h for 16 samples), and 6.25 times fewer hands-on hours compared to serially processing 339 single samples manually (Table 1)); within a work week, this represents 3.2 days of hands-on labor 340 saved. Manual estimates assume no parallelization and are based on the minimum amount of time

341 required to process a single SIP gradient under ideal conditions in our laboratory.

342

343 HT-SIP validation: Hyphosphere soil

344 To demonstrate the HT-SIP pipeline on an important yet challenging sample set (low DNA, low overall 345 enrichment), we targeted hyphosphere soil (the area under direct influence of arbuscular mycorrhizal 346 fungal (AMF) hyphae) using ¹³C labeling of the annual grass Avena barbata in a two-compartment 347 microcosm. After six weeks of labeling, roots in the planted compartment of ¹³C-AMF microcosms were 348 highly enriched (41.3 \pm 1.9 atom% ¹³C). Root biomass in the ¹²C microcosms was unenriched (1.1 \pm 349 0.001 atom% ¹³C). In the no-plant compartment of ¹³C-AMF microcosms, bulk analysis of the soil 350 showed it was slightly enriched $(1.8 \pm 0.1\% \text{ atom}\%^{13}\text{C})$, whereas in the no-AMF control microcosms 351 (where AMF were excluded from the no-plant compartment), the soil ¹³C content was not statistically different from the ¹²C control soil ($1.1 \pm 0.001\%$ versus $1.1 \pm 0.0003\%$, respectively, p < 0.001). This 352 indicates that ¹³CO₂ diffusion into the soil from the labeling chamber headspace was minimal, there was 353

- no significant autotrophic ¹³C-fixation in the no-plant compartment, and that enriched ¹³C detected in the
 hyphosphere was transferred primarily by the AMF hyphae.
- To identify ¹³C enriched metagenome assembled genomes (MAGs) in the hyphosphere, we used the HT-SIP pipeline on DNA extracted from soil-covered hyphal aggregates (termed, "hyphosphere") collected from the no-plant compartment in both ¹³C- and ¹²C-AMF microcosms. SIP density separations of total DNA showed evidence of only slight ¹³C-enrichment, as seen by the small increase in weighted average density (WAD) between ¹²C and ¹³C samples (**Figure 3a**). After mapping the SIP metagenomic reads to the *R. irregularis* genome, we calculated atom percent excess (APE) using qSIP, and found the AMF DNA was significantly ¹³C-enriched (23 atom% ¹³C) (**Figure 3b**).

364 Hyphosphere-qSIP metagenome assembly and binning

365 All fractions were co-assembled using MetaHipMer2, which produced 14.4 assembled Gbp > 1 kb and

366 1.6 assembled Gbp > 10 kb. Compared to single fraction assembly using metaspades, MetaHipMer2

367 produced 3.3 and 3.2 times more assembled Gbp > 1 kb and Gbp > 10 kb, respectively (Supplemental

368 Table S2). We therefore proceeded with the MetaHipMer2 assembly (which did not require bin

dereplication). Overall, 71.2 % of the sequence reads mapped to the MetaHipMer2 assembly. Binning

370 produced 299 medium- and high-quality MAGs; completeness, percent contamination, and MAG genome

- 371 size are available in Supplemental Table S3. Three MAGs were 100% complete, including taxa in the
- 372 orders Cytophagales (mCT1; Bacteroidota), Nitrososphaerales (mCT2; Archaea), and Pedosphaerales
- 373 (mCT3; Verrucomicrobiota). The phyla with the most MAGs assembled were Bacteroidota (68),
- 374 Proteobacteria (51), the candidate phylum radiation Patescibacteria superphylum (50), and Myxococcota

375 (30). On average, $13.3 \pm 7.6\%$ SD of the sequence reads mapped to the MAGs.

376

377 Genomic potential of ¹³C-enriched MAGs in the AMF hyphosphere

378 The soil microbial community in the ¹³C AMF hyphosphere was significantly isotopically enriched; of the

379 299 assembled MAGs, 212 were significantly ¹³C enriched, indicating they consumed plant-fixed ¹³C

transported by the AMF hyphae (Figure 3e). Of these, 43 MAGs were moderately enriched (> 5-10%
APE-¹³C) and 12 MAGs were highly enriched (>10% APE-¹³C), which included 8 Myxococcota MAGs,
a Fibrobacterota from the family UBA11236 (mCT95), an ammonia oxidizing archaeon (AOA) from the
family *Nitrososphaera* (mCT2), and two MAGs from the Verrucomicrobiota family Opitutaceae (mCT7,
mCT160) (Figure 4).

We used comparative genomics of carbohydrate degradation genes (CAZymes), as well as other
genes, to assess possible roles for these MAGs in the microbial food web based on their genomic
potential. Except for the AOA, highly enriched MAGs had multiple homologs of PL6 genes (alginate and
non-alginate polysaccharide lyases [57]) and GH109 genes (glycoprotein α-N-acetylgalactosaminidases)
(Supplemental Table S4); PL6 family enzymes were disproportionately abundant in highly ¹³C-enriched
MAGs (12 of 29 MAGs).

391 Myxococcota are facultative microbial predators that can subsist by predation or saprotrophy 392 [63]. Eight Myxococcota MAGs ranged in APE-¹³C from 12-32%, and seven of these were from the little-393 known Polyangia family Fen-1088 that is known only from metagenomic sequencing (only 31 MAGs in 394 the Genome Taxonomy Database (GTDB)) (accessed June 2022) [64]. Similar to many Myxococcota 395 [65], Fen-1088 have high GC contents (68-71%) and large genome sizes (3.5-7.8 Mbp) (Supplemental 396 Table S3). Three highly-enriched Fen-1088 MAGs (mCT241, mCT215, mCT114) were ca. 10 APE-¹³C 397 more enriched than the AMF and ranged from 30-32% APE-¹³C (Figure 3c, mCT241). Compared to a set 398 of Mycococcota type species genomes [65], these three Fen-1088 MAGs contain similar amounts of 399 genes associated with predation, such as potential cell lysis CAZyme families (7 GH13 genes, 5-7 GH23 400 genes) and protease genes (203-225 MEROPS protease homologs) (Supplemental Table S5). Two of the 401 MAGs contain a chitinase gene (mCT114, mCT215) (Supplemental Table S6). However, these highly 402 enriched MAGs were enriched in glycoside hydrolases and polysaccharide lyases that are atypical for 403 Myxococcota type species [65], such as GH29 (α -fucosidases), GH109 (α -N-acetylgalactosaminidases), 404 GH8 (β -1,4 linkages, such as those found in plant cell walls), PL6 (alginate and non-alginate lyases [66]), 405 and PL14 (lyases of unknown function, including poly(b-mannuronate) lyase). These genomic differences

406 are also apparent across the Myxococcota MAGs from this study, where the highly ¹³C-enriched Fen407 1088 MAGs consistently contained more PL6 and GH29 homologs than less-enriched Myxococcota
408 (Figure 5).

409 Fibrobacterota mCT95 had the same APE as the AMF (23% APE-¹³C) and has chitinolytic

410 potential (9 genes with GH18 domains and 2 genes with GH19 domains, 6 of which were annotated as

411 chitinases (EC 3.2.1.14)). This Fibrobacterota MAG also contained GH74 genes for lysing β-1,4 glucan

412 linkages in plant cell wall polysaccharides.

413 The AOA *Nitrososphaera* mCT2 (**Figure 3d**) was enriched at 12% APE-¹³C and contained genes

414 for ammonia oxidation (amoABC) and nitrite reductase (nirK), as well as the marker gene for the 3-

415 hydroxypropionate/4-hydroxybutyrate cycle for autotrophic C fixation (hydroxybuteryl-CoA dehydratase)

416 [67]. The Nitrososphaera MAG had low glycoside hydrolase content (only 7 genes), no polysaccharide

417 lyase genes, but many glycosyltransferase genes (24 genes).

418 Finally, two Opitutaceae MAGs were 11-12% APE-¹³C enriched. These genomes contained

419 multiple genes with CAZy domains for processing glucose- and galactose-based uronic acids, such as

420 genes for lysing β -1,4 linkages in polyglucuronic acid (PL20), hydrolizing α -1,4 glycosidic linkages in

421 polygalacturonic acid (GH28), and hydrolyzing glucuronic and galacturonic acid monomers (GH105).

422 Polygalacturonases lyse the pectin in plant cell walls [68], while polyglucuronases target the cell walls of

423 bacteria, fungi, and algae [69]. The Opitutaceae MAGs also contained multiple copies of GH29 α-

424 fucosidases. A detailed list of taxonomy and isotopic enrichment for all MAGs is available in

425 Supplemental Table S3, and a comparison of the CAZyme gene content for MAGs with >10% APE-¹³C is

426 available in Supplemental Table S4.

427

429 **DISCUSSION**

430 Stable Isotope Probing is a powerful technique for resolving population demographics, functional traits, 431 and ecological interactions of active microorganisms in situ, without the need for cultivation. However, 432 SIP is not as broadly used as it could be, particularly for sequence-intensive metagenomics and 433 transcriptomics studies, because it is relatively low throughput, time-consuming, and highly manual. 434 Therefore, SIP has rarely been applied with well-replicated, temporally-resolved experimental designs 435 necessary to reveal evolving microbial community activities over space and time. We have created a high 436 throughput semi-automated SIP pipeline, 'HT-SIP', which enables substantially higher sample 437 throughput, reduces labor costs, and makes it more feasible to invest effort in high-risk low-biomass 438 samples that can be used to target the metagenomes of specific function-based subpopulations in complex 439 microbial communities. Since establishing our pipeline (replicated at both LLNL and JGI), we have run 440 more than 1000 samples from a diverse array of sites, including samples from boreal, temperate 441 grassland, agricultural, and tropical forest habitats. This scalable pipeline automates density gradient 442 fractionation, fraction cleanup, and quantification, and we show this method decreases operator time, 443 reduces operator error, and improves reproducibility. Using HT-SIP, we were able to target an important 444 microhabitat, the AMF hyphosphere, and examine potential trophic interactions in the fungal hyphosphere 445 based on ¹³C-enrichment.

446

447 Hyphosphere-SIP: Processing samples with low isotopic enrichment

Assessing a sample's isotopic enrichment (e.g. via mass spectrometry), is often used as a pre-screen factor when deciding whether or not to proceed with SIP density gradient separations, and the number of replicates and SIP fractions to be sequenced. Samples with lower isotopic enrichment require more replicates and fractions to detect taxon-specific enrichment [35]. Based on our soil IRMS data and SIP data alone (**Figure 3a**), we typically would not have proceeded with the hyphosphere samples collected from our ¹³C AMF study, due to their low overall enrichment. However, since AMF are obligate biotrophs and the plant biomass was highly ¹³C enriched, we hypothesized that AMF hyphae and their

455	surrounding hyphosphere might also be enriched, and that the low bulk ¹³ C hyphosphere value might have
456	been caused by dilution from a large ¹² C soil background, along with our inability to physically sample
457	this microhabitat precisely. We thus proceeded with a DNA-SIP strategy of sequencing all fractions (14
458	total) to increase the chance of detecting enriched taxa. While initial IRMS data and total DNA-SIP
459	separations suggested SIP might be impracticable on these samples due to insufficient ¹³ C label, instead,
460	taxon-specific qSIP indicated a highly enriched ¹³ C-AMF signal.

461

462 Dissecting trophic interactions in the AMF hyphosphere

463 Paradoxically, AMF are capable of stimulating decomposition of SOM and detritus [37, 38], but do not

464 have the enzymatic repertoire to decompose SOM themselves. We and others have hypothesized that

465 AMF collaborate with their soil microbiome to mineralize organic nutrients [43]; previous research shows

the presence of AMF modifies the litter-decomposing microbiome [38] and the hyphosphere microbiome

467 synergistically increases the amount of nitrogen AMF transfer back to the plant host [70]. The ¹³C-AMF

468 hyphosphere MAGs we identified in this study are a key advance, enabling us to test hypotheses related to

469 these phenomena and determine the molecular mechanisms that underpin them. Because SIP-

470 metagenomes target DNA from active organisms that recently consumed an isotopically-labeled substrate,

471 their genomic content represents the machinery that runs the microbial food web and provides a means to

472 dissect potential trophic interactions.

473

474 *Predation in the hyphosphere*

475 Using qSIP-estimated MAG atom percent excess, we examined potential trophic interactions in the fungal

476 hyphosphere based on ¹³C-enrichment. Intriguingly, Myxococcota from the poorly-characterized family

477 Fen-1088 were the most enriched taxa detected in the hyphosphere. While Myxococcota are a known

478 component of AMF hyphosphere communities [71], their functional role has not been previously

479 determined. The particularly high atom percent ¹³C enrichment of the Fen-1088 family suggests they are

480 either directly feeding upon C exuded by the AMF, or are predators which target AMF hyphae or other

481 microbes in the AMF hyphosphere. The Myxococcota phylum contains many facultative predators that 482 can subsist by consuming microbial or plant organic matter [63], and have a broad prey range including 483 bacteria and fungi [72, 73]. Since our Myxococcota MAGs have high GC content and large genomes, it is 484 unlikely that they are AMF endosymbionts, which often have reduced genomes. Previous GWAS analysis 485 indicates that Myxococcota have many prey-specific genes, rather than a general set of antimicrobial 486 genes, which likely enable them to target a broad prey range [74]. Our analysis of the Fen-1088 MAGs 487 also points to a large arsenal of proteases that may be used to consume prey, these are also found in many 488 Myxococcota type species [65]. However, the relative lack of GH18 chitinase genes suggests this family 489 may not be chitinolytic or may have low chitin degradation efficiency, as highly efficient chitinolytic 490 organisms are thought to produce multiple types of chitinases [75, 76]. 491 While the Fen-1088 MAGs are similar to other Myxococcota genomes, in that they contain a 492 large array of CAZymes for carbohydrate and polysaccharide degradation, they also contain multiple 493 copies of genes with CAZyme domains that are uncommon in Myxococcota type species. Most of these 494 CAZymes are hypothetical proteins, but the presence of these CAZyme domains hints at potential 495 function. We consistently found two enzyme groups, GH29 and PL6, in Fen-1088 MAGs. The GH29 496 group is known to contain alpha-fucosidases, which remove terminal L-fucoses from oligosaccharides or 497 their conjugates [77]. Many biomolecules are fucosylated [78] — polysaccharides, glycoproteins, and 498 glycolipids can have attached fucoses [77]. AMF hyphae are well-known for exuding glycoproteins and 499 related compounds, that appear to play a key role in soil carbon stabilization. Fucose can be exuded and 500 tightly attached to the AMF hyphal surface; in one previous study, fucose represented 3.5-5% of the mass 501 of poly- and mono-saccharides that were exuded or could be gently hydrolyzed from the fungal surface 502 [79]. Rhizophagus irregularis also exudes fucosylated lipo-chitooligosaccharides [80], which may be 503 signaling molecules used when establishing a symbiosis with a plant host [81]. 504 Much less is known about polyspecific enzyme family PL6; these enzymes are abundant in Fen-505 1088, and in all our MAGs with >10% APE-¹³C except the AOA MAG. PL6 contains alginate lyases and 506 non-alginate lyases [66] that cleave $\beta(1-4)$ linkages within polysaccharides built from mannuronic and

507 guluronic acids [66], such as alginate produced by brown algae and some bacteria, or between these acids 508 and other building blocks for non-alginates. While these polysaccharides have been detected in soil, their 509 origin is difficult to determine. Bacteria in the genera Pseudomonas and Azotobacter species can produce 510 a bacterial form of alginate [82]. Little is known about the composition of mycorrhizal exo- and endo-511 polysaccharides, so it is not possible to rule out that these enzymes are acting on an AMF-produced 512 polysaccharide. Mannose, the sugar from which mannuronic acid is built, is abundant in the mono- and 513 polysaccharides bound to the surface of AMF hyphae [79], but we have no information about how these 514 monosaccharides are polymerized. Further research on both the polysaccharides in the AMF hyphosphere 515 and the feeding preferences of the Fen-1088 Myxococcota are needed to determine the nature of this 516 relationship. 517 Stable isotope measurements can benefit food web studies, where the ¹³C enrichment of an 518 organism is used as a conservative indicator of the 13 C enrichment of the substrate they consume [29, 83]. 519 In some cases, predators can be more enriched than their prey. For example, in a previous qSIP study, 520 viral DNA was more ¹³C-enriched than the microbial host, likely because the host was using more 521 recently assimilated C to support viral replication [34]. Similarly, in a recent qSIP meta-analysis, 522 predators assimilated ¹⁸O or ¹³C at higher rates than non-predators [29]. We note that isotopic 523 concentration by predators due to isotopic fractionation (ca. 1 per mil per trophic level for C [83]) is not 524 relevant to our study, where we have used tracer levels of isotope enrichment. In our study, the Fen-1088 525 MAGs were more ¹³C enrichment than the AMF, even though AMF were the only source of ¹³C in the no-526 plant compartment. Myxococcota likely became more enriched than the mean AMF enrichment by 527 consuming ¹³C-rich compounds recently transported from the plant host, such as newer hyphae or fresh 528 exudates. At the time of harvest, plant root bulk enrichment was 41 atom% and AMF hyphae were 23 529 atom% (estimated by qSIP), but we expect that recently produced hyphae had a higher isotopic signature, 530 more similar to the plant host (i.e. DNA extracted from all present AMF biomass would include hyphae produced earlier part of the ${}^{13}CO_2$ labeling period when the plant was less ${}^{13}C$ enriched). 531

533 Interactions between AMF and ammonia oxidizing archaea (AOA)

534 The relatively high ¹³C enrichment of the Nitrosophaera MAG (12 APE ¹³C) suggests this AOA was 535 intimately associated with the AMF, or nearby biota that obtained substantial quantities of ¹³C from the 536 AMF (e.g., Fibrobacterota, Opitituceae, Myxococcota). While AOA are dominantly autotrophic, there is 537 some evidence they can use organic C [84-86]. Because we did not detect ¹³C enrichment in soil from 538 hyphae-free controls, it is unlikely non-specific subsurface diffusion of ¹³CO₂ gas contributed to 539 autotrophic ¹³C assimilation. Therefore, we conclude that AMF played a key role in the transport of plant 540 photosynthate C to the AOA—either through direct (AMF \rightarrow AOA) or indirect (AMF \rightarrow other biota \rightarrow 541 AOA) pathways. 542 The nature of multitrophic interactions between AMF, AOA, and other soil biota remains largely

543 unknown. AMF can induce changes in AOA community structure [87], with positive, negative, and

negligible effects on AOA abundance [87-90]. Positive interactions between AMF and AOA may be

545 driven by C supply or hyphosphere soil acidification. Low soil pH promotes AOA abundance and activity

546 [84]. Negative interactions may be driven by competition for ammonia, which can suppress the AOA

547 community [88], although this antagonistic relationship may be alleviated in N-rich soil [90]. Because

548 AOA play an important role in the first step of nitrification [85, 91], AMF effects on AOA abundance and

549 activity have implications for terrestrial N cycling and N₂O emissions.

550

551 Interactions between AMF and decomposers that can potentially degrade fungal or plant biomass

AMF hyphae turnover quickly (5-6 days, [92]) and cycling of this necromass represents a potentially

rapid flow of nutrients and photosynthate C into a large volume of the soil system [43, 93]. Our study's

highly ¹³C-enriched MAGs have the genomic potential to degrade AMF fungal biomass. All of the

555 enriched taxa contain GH109 genes, whose primary reported activity is α-N-acetylgalactosaminidase

556 (additional functions may be as yet unknown). Galactose is a component of polysaccharides attached to

- 557 the surface of AMF hyphae [79], and a lectin specific to D-galactose or N-acetyl-D-galactosamine
- 558 glycoproteins was able to bind strongly to protein extracted from AMF [94]. In particular, Fibrobacterota

mCT95 has 11 putative chitinase genes (GH18, GH19) and appears to be deriving most of its C from the AMF (mCT95 has the same APE- 13 C as the AMF), and thus could be performing a chitinolytic function in this soil food web.

562 All the highly enriched MAGs and many of the low- to medium-enriched MAGs have 563 enzymatic potential to degrade components of plant biomass. The MAGs from Fibrobacterota and 564 Verrucomicrobiota family Opitutaceae have isolated relatives that are thought to be involved in 565 decomposition. Fibrobacterota include cellulose degrading bacteria found in mammal rumens [95], 566 termite guts [96], anaerobic cellulose reactors [97], and rice paddy soil [98]. The Verrucomicrobiota 567 family Opitutaceae contains isolates derived from rice patties and insect guts [99-102]. In our previous 568 study decomposition gene expression in the rhizosphere and detritusphere using metatranscriptomics, we 569 found that Fibrobacterota and Opitutaceae were two of the three groups that exhibited the highest 570 decomposition gene expression when both root exudates and detritus were available [103]. Further 571 examination would be required to determine if the MAGs from this study exhibit similar synergistic 572 behavior in the AMF hyphosphere, and whether this stimulates the decomposition of plant residues.

573

574 Methodological considerations: SIP DNA recovery

575 The amount of DNA recovered in each SIP density fraction can be a limiting factor for library 576 construction, especially in the highest and lowest density fractions where only a small portion of total 577 DNA is captured. In our research, we typically aim for 100 ng DNA per fraction, so that 20 ng may be 578 reserved for 3 analyses: metagenomic sequencing, 16S rRNA gene and ITS amplicon libraries, and qPCR 579 assays. To reliably achieve ~ 100 ng DNA in the majority of the fractions collected, we typically 580 recommend loading $3-5 \mu g$ of DNA, because not all DNA added to the density centrifuge tube is 581 recovered after fraction collection and desalting. Prior to adding non-ionic detergents, we noticed that 582 DNA recovery appeared to be correlated with the initial amount loaded and hypothesized that DNA was 583 being lost by an adsorption mechanism. Adsorption of DNA to polypropylene tube walls can potentially 584 lead to substantial sample loss, especially when DNA is in a high ionic strength solution [48], such as

CsCl gradient buffer. Our tests indicate that adding a low concentration of Tween-20 (0.0001%) leads to a near doubling of DNA yield. Adding Tween-20 may be particularly critical when limited DNA is available, such as from small samples or low biomass environments. Using this method, samples with 1 µg DNA and below can be more reliably processed and analyzed using metagenomic sequencing technologies that have low DNA input requirements. Here, we successfully analyzed 350 ng DNA per hyphosphere DNA sample with a 42% DNA recovery, which was suitable for metagenomic sequencing of the fractions containing DNA.

592

593 HT-SIP optimization

594 Automating the SIP process significantly decreased the required operator hours (Table 1) while 595 simultaneously improving reproducibility and sample recovery. Traditionally, after manually 596 fractionating a density gradient, an additional 1-2 hours per sample is required to desalt gradient fractions 597 (nucleic acid purification). Thus, in many research groups, a maximum of 6-8 samples may be processed 598 per week, a grueling prospect if this pace is kept up week after week. HT-SIP makes it possible to 599 routinely process 16 samples on a weekly basis, since the overall time to process a group of samples is 600 decreased by over half, and the laborious "hands-on" tasks are significantly decreased by one-sixth. These 601 time savings also translate into substantial labor cost savings, which over time can offset the initial cost of 602 purchasing robotic instruments.

603 In the process of assessing different time saving methods, we attempted different techniques that 604 were not adopted as part of the final pipeline, but these experiences may benefit others when developing 605 their own pipelines. In addition to PEG precipitation, we attempted magbead cleanups, which are more 606 time efficient than PEG if multiple magnetic plates are run in parallel; however in our hands, we found 607 that PEG precipitations had higher yields. We also assessed if DNA intercalators could be used to 608 minimize density differences associated with differences in GC content, with the goal of minimizing the 609 need for separate 12C controls. Actinomycin D has been shown to reduce the native buoyant density of 610 DNA with greater effect in GC rich DNA [104], thus theoretically reducing 90% of natural density

differences. We found that the high concentrations needed to reduce the density of GC rich DNA alsoreduced the quality of the DNA density distribution and the overall DNA recovery. While we did not

613 pursue further use of intercalators, with some optimization this could be a viable approach. These two

- 614 protocols are available in the Supplemental Methods.
- 615

616 CONCLUSIONS

617 Increasing the throughput of SIP is needed to promote well-replicated ecological scale studies to

618 determine the ecophysiology of uncultivated organisms in complex environments. Here, we demonstrated

619 an automation approach to expedite the most tedious tasks for SIP—fractionation, cleanup,

620 quantification—that can increase the throughput and decrease the variability of SIP, with DNA recovery

621 that is comparable to manual SIP processing. Decreasing the hands-on labor needed to run SIP samples

622 inherently makes high-risk samples more feasible, such as the AMF hyphosphere samples we analyzed,

623 where we had limited soil volume, low bulk atom percent enrichment and minimal separation based on

total DNA density curves. The highly ¹³C-enriched hyphosphere MAGs identified in this study highlight

625 the potential for trophic interactions in this zone, which includes predation, decomposition of fungal or

626 plant biomass, and ammonia oxidation. In combination with other '-omics technologies, such as

627 metatranscriptomics or proteomics, these MAGs will provide an important genomic resource for future

628 experiments exploring interactions between AMF and their native microbiome.

629

630 ACKNOWLEDGEMENTS

631 We thank Steve Kubala for assistance programming the robotic methods, Craig See for assistance with

632 manual refractometry, G. Mike Allen for SIP technical assistance, and the JGI IMG and metagenomics

633 teams for assistance with data processing (Neha Varghese, Alicia Clum, Marcel Huntemann, Tatiparthi

634 Reddy, Supratim Mukherjee). Development of the HT-SIP pipeline was sponsored by the Joint Genome

635 Institute through an Emerging Technologies Opportunities Program award (DOI:

636 10.46936/10.25585/60008401) to J.P.R. Testing of experimental samples on the LLNL HT-SIP pipeline

- 637 was supported by the U.S. Department of Energy Office of Science, Office of Biological and
- 638 Environmental Research (BER) Genomic Science Program (GSP) 'Microbes Persist' Scientific Focus
- 639 Area award SWC1632 to J.P.R. The ¹³CO₂ plant-AMF experiment was supported by DOE BER GSP
- awards DE-SC0016247 and DE-SC0020163 to M.K.F, and hyphosphere-SIP metagenomics sequencing
- and analysis was supported by DOE BER Early Career award SCW1711 to E.E.N. Work at Lawrence
- 642 Livermore National Laboratory was conducted under the auspices of the U.S. DOE under Contract DE-
- 643 AC52-07NA27344. The work conducted by the U.S. Department of Energy Joint Genome Institute
- 644 (<u>https://ror.org/04xm1d337</u>), a DOE Office of Science User Facility, is supported by the Office of Science
- of the U.S. Department of Energy operated under Contract No. DE-AC02-05CH11231.
- 646

647 **CONFLICTS OF INTEREST**

- 648 The authors declare no conflicts of interest.
- 649

650 FIGURE CAPTIONS

651 Figure 1. Comparison of manual versus automated fractionation of SIP density gradients.

652 Fractionation is the process of dividing a SIP density gradient into multiple fractions, where the initial 653 fractions at the bottom of the tube are the heaviest and the final fractions at the top of the tube are the 654 lightest. Buoyant density (g/ml) for each fraction is measured via refractometry and is represented by a 655 single dot. (A) For "manual" fractionation, 22 independent density gradients were fractionated by visually 656 counting and collecting droplets in microcentrifuge tubes using the method described in Blazewicz et al 657 [17]. The number of fractions collected from manual density gradient was variable (range 15-27 fractions 658 per gradient); only fractions 2-19 are displayed. (B) For automated fractionation, 24 independent density 659 gradients were fractionated robotically using an Agilent Technologies fraction collector, which 660 automatically divides the gradients into fractions of a set volume ($\sim 236 \mu$) and dispenses them into a 96-661 well plate. Automated density gradients consistently produced 22 fractions per gradient. Fractions at the 662 beginning and end of the gradient (fractions 1, 20-22) were excluded as these densities are altered by the 663 water used to displace the gradient and are not typically used for molecular analysis.

664

665 Figure 2. DNA recovery comparison for manual and semi-automated PEG precipitation methods, 666 and the impact of adding a non-ionic detergent (Tween-20) to the SIP gradient buffer. After a 667 density gradient is fractionated, each fraction needs to be desalted prior to quantification and sequencing 668 analysis, which can be accomplished using nucleic acid precipitations. (A) We compared "manual" PEG 669 precipitations (n=3 SIP gradients), where each fraction is precipitated in microcentrifuge tubes by an 670 individual (as per Blazewicz et al. [17]), and semi-automated or "robot" PEG precipitations (n=3 SIP 671 gradients), where a Hamilton STAR liquid handling robot performs the precipitations in 96-well plates. 672 This process is semi-automated because some steps require assistance from an individual (e.g., 673 transferring plates to a centrifuge for DNA sedimentation). (B) We tested how adding Tween-20 to the 674 density gradient mixture impacts DNA recovery for a large SIP experiment analyzing soil DNA; all 675 samples were processed semi-automatically by the robot. Tween-20 was added to a subset of the samples

676 (+Tween, n = 38 SIP gradients) or processed using our standard density gradient buffer without Tween-20 677 (-Tween, n = 63 SIP gradients). Both experiments were conducted using 4 µg soil DNA per SIP gradient; 678 recovery was calculated by summing recovered DNA (measured by Picogreen) in the recovered density 679 fractions post-cleanup and dividing by the initial DNA input. Error bars represent the standard error of the 680 mean.

681

682 Figure 3: ¹³C-Hyphosphere Metagenome Assembled Genomes (MAGs) isolated by SIP-

683 metagenomics. Concentration versus fraction density of (A) total DNA extracted and SIP fractionated

from a ¹³C-hyphosphere soil (red lines) and ¹²C-hyphosphere control soil (blue lines); n=3. Dashed lines

are the weighted average density (WAD) of the DNA of the replicate gradients for each isotope. Within

686 this gradient, we used qSIP to estimate taxon-specific DNA masses for (B) the AMF host *Rhizophagus*

687 *intraradices*, and two MAGs recovered from the AMF hyphosphere: (C) a Myxococcota MAG

688 (mCT241_Fen-1088) (the most ¹³C-enriched organism detected), and **(D)** an archaeal ammonia oxidizer

689 (mCT2_*Nitrososphaera*). Taxon-specific DNA masses were estimated by multiplying a fraction's total

690 DNA mass by taxon relative abundance (e.g., MAG counts divided by metagenomic library counts). (E)

691 Estimated median atom percent excess (APE) of all assembled MAGs, which were calculated based on

692 the difference in weighted average density between ¹³C-hyphosphere samples and ¹²C-hyphosphere

693 control samples. Red bars indicate the 212 MAGs that had significantly greater ¹³C enrichment than 0

694 (lower 90% CI bound greater than 0), and blue bars indicate the MAGs that were unenriched (lower 90%

695 CI bound below 0). The dashed gray line indicates the APE of the AMF, *Rhizophagus intraradices*, which

696 supplied ¹³C to the hyphosphere chamber. Taxa are grouped by phylum, and letters indicate the APE of

697 the taxa shown in panels B-D.

698

699 Figure 4: Ranked enrichment of highly enriched MAGs in the AMF ¹³C-hyphosphere, as estimated

700 by qSIP. MAGs displayed have >5% atom percent excess (APE) ¹³C and are colored by phylum

affiliation. Dashed line indicates the APE-¹³C of the AMF, *Rhizophagus intraradices*. Error bars represent

the 90% confidence interval. A full list of MAGs and their isotopic enrichment is available in

703 Supplemental Table 3.

704

705 Figure 5: Genomic comparison of CAZy family homologs identified in Myxococcota MAGs

- assembled in this study. Rows indicate the number of gene homologs (red-blue color scale) detected per
- 707 CAZy family, columns indicate the associated MAGs. Atom percent excess ¹³C (APE-¹³C) estimated by
- 708 qSIP is presented in the top row (yellow-purple-black color scale). Columns and rows were clustered
- vising one-dimensional hierarchical clustering based on genomic content. CAZy families displayed had
- significantly more or less genes detected in the Fen-1088 MAGs compared to the rest of the Myxococcota
- 711 MAGs (student's t-test, p <0.05); full results are available in Supplemental Table S6. Acronyms: GH =
- 712 glycoside hydrolase; PL = polysaccharide lyase; CBM = carbohydrate binding module; GT =
- 713 glycosyltransferase; AA = auxiliary activity.

SIP Processing Steps	Manual Time (hours)		Automated Time (hours)	
	Hands-on	Total	Hands-on	Total
Fraction Collection	1	1	0.2	0.6
Sample Cleanup	0.4	1	0.04†	0.5†
DNA Quantification	0.5	0.6	0.06†	0.13†
Total Time (per 1 sample)	1.9	2.6	0.3†	1.2†
Batch Time (per 16 samples)	30	42	4.8	20

715	Table 1. Time comparison for manual versus automated SIP fractionation, cleanup, and DNA
716	quantification. Estimates are based on processing 22 fractions per SIP tube. The "Hands-on" columns
717	indicate the time an individual must actively manipulate the samples, while "total" columns indicate the
718	total time required for the entire process. Manual cleanup and quantification time estimates are based on
719	processing a single SIP gradient and assume maximum processing speed. Automated fraction cleanup
720	time is based on the time required to fractionate a single tube using the Agilent Infinity Fraction
721	Collector. Automated sample cleanup and DNA quantification times are based on the processing times for
722	the Hamilton STAR liquid handling robots. The † symbol indicates that 16 SIP gradients are processed
723	simultaneously in 4 plates (4 gradients per plate), and the "per 1 sample" times are calculated by dividing
724	the total time by 16. "Batch" processing times are the times required to process 16 density gradients.
725	

726 **REFERENCES**

- Slysz GW, Steinke L, Ward DM, Klatt CG, Clauss TR, Purvine SO, et al. Automated
 data extraction from in situ protein-stable isotope probing studies. Journal of proteome
 research. 2014;13(3):1200-10.
- 731 2. Radajewski S, Ineson P, Parekh NR, Murrell J. Stable-isotope probing as a tool in microbial ecology. Nature. 2000;403(10):646-9.
- Manefield M, Whiteley AS, Griffiths R, Bailey MJ. RNA Stable Isotope Probing, a
 Novel Means of Linking Microbial Community Function to Phylogeny. Appl Environ
 Microbiol. 2002.
- Baran R, Reindl W, Northen TR. Mass spectrometry based metabolomics and enzymatic
 assays for functional genomics. Curr Opin Microbiol. 2009;12(5):547-52; doi: https://doi.org/10.1016/j.mib.2009.07.004.
- 5. Dumont MG, Hernández García M. Stable Isotope Probing: Methods and Protocols.
 Totowa, NJ, US: Humana Press; 2019.
- Koch BJ, McHugh TA, Hayer M, Schwartz E, Blazewicz SJ, Dijkstra P, et al. Estimating
 taxon-specific population dynamics in diverse microbial communities. Ecosphere.
 2018;9(1); doi: 10.1002/ecs2.2090.
- 744
 7. Pett-Ridge J, Weber PK. NanoSIP: NanoSIMS application for microbial biology. 2nd
 redn: Humana Press; 2021.
- 8. Murrell JC, Whiteley AS. Stable Isotope Probing and Related Technologies. Washington
 DC: ASM Press; 2011.
- Pepe-Ranney C, Campbell AN, Koechli CN, Berthrong S, Buckley DH. Unearthing the
 Ecology of Soil Microorganisms Using a High Resolution DNA-SIP Approach to
 Explore Cellulose and Xylose Metabolism in Soil. Front Microbiol. 2016;7(94):626; doi:
 10.3389/fmicb.2016.00703.
- Rangel-Castro JI, Killham K, Ostle N, Nicol GW, Anderson IC, Scrimgeour CM, et al.
 Stable isotope probing analysis of the influence of liming on root exudate utilization by
 soil microorganisms. Environmental Microbiology. 2005;7(6):828-38; doi:
 10.1111/emi.2005.7.issue-6.
- Vandenkoornhuyse P, Mahé S, Ineson P, Staddon P, Ostle N, Cliquet J-B, et al. Active
 root-inhabiting microbes identified by rapid incorporation of plant-derived carbon into
 RNA. Proc Natl Acad Sci USA. 2007;104(43):16970-5; doi: 10.1073/pnas.0705902104.
- 12. Sieradzki ET, Morando M, Fuhrman JA. Metagenomics and Quantitative Stable Isotope
 Probing Offer Insights into Metabolism of Polycyclic Aromatic Hydrocarbon Degraders
 in Chronically Polluted Seawater. mSystems. 2021;6(3):e00245-21; doi:
- 762 10.1128/msystems.00245-21 PMID 33975968.
- Neufeld JD, Schäfer H, Cox MJ, Boden R, McDonald IR, Murrell JC. Stable-isotope
 probing implicates Methylophaga spp and novel Gammaproteobacteria in marine
 methanol and methylamine metabolism. ISME J. 2007;1(6):480-91; doi:
 10.1038/ismej.2007.65 PMID 18043650.
- 76714.Jia Z, Conrad R. Bacteria rather than Archaea dominate microbial ammonia oxidation in768an agricultural soil. Environ Microbiol. 2009; doi: 10.1111/j.1462-2920.2009.01891.x.
- 15. Buckley D, Huangyutitham V, Hsu S, Nelson T. Stable Isotope Probing with 15N2
- 770 Reveals Novel Noncultivated Diazotrophs in Soil. Appl Environ Microbiol.
- 771 2007;73(10):3196-204; doi: 10.1128/AEM.02610-06.

772	16.	Angel R, Panhölzl C, Gabriel R, Herbold C, Wanek W, Richter A, et al. Application of
773		stable-isotope labelling techniques for the detection of active diazotrophs. Environ
774		Microbiol. 2018;20(1):44-61; doi: 10.1111/1462-2920.13954 PMID - 29027346.
775	17.	Blazewicz SJ, Schwartz E, Firestone MK. Growth and death of bacteria and fungi
776		underlie rainfall-induced carbon dioxide pulses from seasonally dried soil. Ecology.
777		2014;95(5):1162-72.
778	18.	Blazewicz SJ, Hungate BA, Koch BJ, Nuccio EE, Morrissey E, Brodie EL, et al. Taxon-
779		specific microbial growth and mortality patterns reveal distinct temporal population
780		responses to rewetting in a California grassland soil. ISME J. 2020;14(6):1520-32; doi:
781		10.1038/s41396-020-0617-3.
782	19.	Barnett SE, Youngblut ND, Buckley DH. Stable Isotope Probing, Methods and Protocols.
783		Methods in Molecular Biology. 2019;2046:109-28; doi: 10.1007/978-1-4939-9721-3_9
784		PMID - 31407300.
785	20.	Hungate BA, Mau RL, Schwartz E, Caporaso JG, Dijkstra P, Van Gestel N, et al.
786		Quantitative Microbial Ecology Through Stable Isotope Probing. Appl Environ
787		Microbiol. 2015; doi: 10.1128/AEM.02280-15
788	21.	Blazewicz SJ, Schwartz E. Dynamics of (18)O incorporation from H2(18) O into soil
789		microbial DNA. Microb Ecol. 2011;61(4):911-6; doi: 10.1007/s00248-011-9826-7.
790	22.	Schwartz E, Hayer M, Hungate BA, Koch BJ, McHugh TA, Mercurio W, et al. Stable
791		isotope probing with 18O-water to investigate microbial growth and death in
792		environmental samples. Curr Opin Biotechnol. 2016;41:14-8; doi:
793		10.1016/j.copbio.2016.03.003 PMID - 27035052.
794	23.	Trubl G, Kimbrel JA, Liquet-Gonzalez J, Nuccio EE, Weber PK, Pett-Ridge J, et al.
795		Active virus-host interactions at sub-freezing temperatures in Arctic peat soil.
796	24	Microbiome. 2021;9(1):208; doi: 10.1186/s40168-021-01154-2 PMID - 34663463.
797	24.	Morrissey EM, Mau RL, Hayer M, Liu X-JA, Schwartz E, Dijkstra P, et al. Evolutionary
798 700		history constrains microbial traits across environmental variation. Nat Ecol Evol.
799	25	2019;3(7):1064-9; doi: 10.1038/s41559-019-0918-y PMID - 31209289.
800	25.	Li J, Mau RL, Dijkstra P, Koch BJ, Schwartz E, Liu X-JA, et al. Predictive genomic traits
801		for bacterial growth in culture versus actual growth in soil. ISME J. 2019;13(9):2162-72;
802	26	doi: 10.1038/s41396-019-0422-z PMID - 31053828.
803	26.	Wang C, Morrissey EM, Mau RL, Hayer M, Piñeiro J, Mack MC, et al. The temperature
804 805		sensitivity of soil: microbial biodiversity, growth, and carbon mineralization. ISME J.
805 806	27.	2021;15(9):2738-47; doi: 10.1038/s41396-021-00959-1 PMID - 33782569. Purcell AM, Hayer M, Koch BJ, Mau RL, Blazewicz SJ, Dijkstra P, et al. Decreased
800 807	27.	
		growth of wild soil microbes after 15 years of transplant-induced warming in a montane meadow. Global Change Biol. 2022;28(1):128-39; doi: 10.1111/gcb.15911 PMID -
808 809		34587352.
809	28.	Stone BW, Li J, Koch BJ, Blazewicz SJ, Dijkstra P, Hayer M, et al. Nutrients cause
810	20.	consolidation of soil carbon flux to small proportion of bacterial community. Nat
812		Commun. 2021;12(1):3381; doi: 10.1038/s41467-021-23676-x PMID - 34099669.
812	29.	Hungate BA, Marks JC, Power ME, Schwartz E, Groenigen KJv, Blazewicz SJ, et al. The
813	29.	Functional Significance of Bacterial Predators. mBio. 2021;12(2):e00466-21; doi:
815		10.1128/mbio.00466-21 PMID - 33906922.
816	30.	Wilhelm RC, Pepe-Ranney C, Weisenhorn P, Lipton M, Buckley DH. Competitive
817	50.	Exclusion and Metabolic Dependency among Microorganisms Structure the Cellulose
01/		Zierzeiten and Frederone Dependency among Frieroorganisms Structure and Schuldbe

818		Economy of an Agricultural Soil. mBio. 2021;12(1); doi: 10.1128/mbio.03099-20 PMID
819	21	- 33402535.
820	31.	Greenlon A, Sieradzki E, Zablocki O, Koch BJ, Foley MM, Kimbrel JA, et al.
821		Quantitative stable-isotope probing (qSIP) with metagenomics links microbial physiology
822		and activity to soil moisture in Mediterranean-climate grassland ecosystems. bioRxiv.
823	22	2022:2022.05.02.490339; doi: 10.1101/2022.05.02.490339.
824	32.	Eyice Ö, Namura M, Chen Y, Mead A, Samavedam S, Schäfer H. SIP metagenomics
825		identifies uncultivated Methylophilaceae as dimethylsulphide degrading bacteria in soil
826		and lake sediment. ISME J. 2015;9(11):2336-48; doi: 10.1038/ismej.2015.37 PMID -
827	22	25822481.
828	33.	Barnett SE, Youngblut ND, Koechli CN, Buckley DH. Multisubstrate DNA stable
829		isotope probing reveals guild structure of bacteria that mediate soil carbon cycling. Proc
830		Natl Acad Sci USA. 2021;118(47):e2115292118; doi: 10.1073/pnas.2115292118 PMID -
831	24	34799453.
832	34.	Starr EP, Shi S, Blazewicz SJ, Koch BJ, Probst AJ, Hungate BA, et al. Stable-Isotope-
833		Informed, Genome-Resolved Metagenomics Uncovers Potential Cross-Kingdom
834		Interactions in Rhizosphere Soil. Msphere. 2021;6(5):e00085-21; doi:
835	25	10.1128/msphere.00085-21 PMID - 34468166.
836	35.	Sieradzki ET, Koch BJ, Greenlon A, Sachdeva R, Malmstrom RR, Mau RL, et al.
837		Measurement Error and Resolution in Quantitative Stable Isotope Probing: Implications
838		for Experimental Design. mSystems. 2020;5(4):e00151-20; doi:
839	26	10.1128/msystems.00151-20 PMID - 32694124.
840	36.	Smith SE, Read DJ. Mycorrhizal Symbiosis. New York: Academic Press; 2008.
841	37.	Barea JM, Azcon R, Azcon-Aguilar C. Mycorrhizosphere interactions to improve plant
842		fitness and soil quality. Antonie Van Leeuwenhoek International Journal of General and
843	20	Molecular Microbiology. 2002;81(1-4):343-51; doi: 10.1023/a:1020588701325.
844	38.	Nuccio EE, Hodge A, Pett-Ridge J, Herman DJ, Weber PK, Firestone MK. An arbuscular
845		mycorrhizal fungus significantly modifies the soil bacterial community and nitrogen
846		cycling during litter decomposition. Environ Microbiol. 2013;15(6):1870-81; doi:
847	20	10.1111/1462-2920.12081.
848	39.	Kakouridis A, Hagen JA, Kan MP, Mambelli S, Feldman LJ, Herman DJ, et al. Routes to
849		Roots: Direct Evidence of Water Transport by Arbuscular Mycorrhizal Fungi to Host
850 851	40	Plants. New Phytol. 2022; doi: 10.1111/nph.18281 PMID - 35633108.
851	40.	Hodge A, Campbell CD, Fitter AH. An arbuscular mycorrhizal fungus accelerates
852		decomposition and acquires nitrogen directly from organic material. Nature.
853	41	2001;413(6853):297-9.
854 855	41.	Atul-Nayyar A, Hamel C, Hanson K, Germida J. The arbuscular mycorrhizal symbiosis
855 856		links N mineralization to plant demand. Mycorrhiza. 2009;19(4):239-46; doi: 10.1007/s00572-008-0215-0.
850 857	42.	Cheng L, Booker FL, Tu C, Burkey KO, Zhou L, Shew HD, et al. Arbuscular
858	42.	mycorrhizal fungi increase organic carbon decomposition under elevated CO2. Science.
858 859		
	12	2012;337(6098):1084-7; doi: 10.1126/science.1224304.
860 861	43.	Frey SD. Mycorrhizal Fungi as Mediators of Soil Organic Matter Dynamics. Annu Rev Ecol, Evol Syst. 2019;50:237-59.
862	44.	Herman DJ, Firestone MK, Nuccio E, Hodge A. Interactions between an arbuscular
862	77.	mycorrhizal fungus and a soil microbial community mediating litter decomposition.
005		mycorrinzar rangus and a son microorar community mediating nucr accomposition.

864		FEMS Microbiology Ecology. 2012;80(1):236-47; doi: 10.1111/j.1574-
865		6941.2011.01292.x.
866	45.	Dodd JC, Boddington CL, Rodriguez A, Gonzalez-Chavez C, Mansur I. Mycelium of
867		Arbuscular Mycorrhizal fungi (AMF) from different genera: form, function and
868		detection. Plant Soil. 2000;226(2):131-51; doi: 10.1023/a:1026574828169.
869	46.	Buckley DH, Huangyutitham V, Hsu S-F, Nelson TA: Stable Isotope Probing with 15N2
870		Reveals Novel Noncultivated Diazotrophs in Soil. In: Applied and Environmental
871		Microbiology. vol. 73; 2007: 3196-204.
872	47.	Neufeld JD, Vohra J, Dumont MG, Lueders T, Manefield M, Friedrich MW, et al. DNA
873		stable-isotope probing. Nature Protocols. 2007;2(4):860-6; doi: 10.1038/nprot.2007.109
874		PMID - 17446886.
875	48.	Gaillard C, Strauss F. Avoiding adsorption of DNA to polypropylene tubes and
876		denaturation of short DNA fragments. Technical Tips Online. 1998;3(1):63-5; doi:
877		10.1016/s1366-2120(08)70101-6.
878	49.	Garvin AM, Fritsch A. Purifying and Concentrating Genomic DNA from Mock Forensic
879		Samples Using Millipore Amicon Filters. J Forensic Sci. 2013;58(s1):S173-S5; doi:
880		10.1111/1556-4029.12002 PMID - 23082821.
881	50.	Illumina. NextSeq 1000 and 2000 Denature and Dilute Libraries Guide (1000000139235
882		v3).
883	51.	Hofmeyr S, Egan R, Georganas E, Copeland AC, Riley R, Clum A, et al. Terabase-scale
884		metagenome coassembly with MetaHipMer. Scientific Reports. 2020;10(1):10689; doi:
885		10.1038/s41598-020-67416-5 PMID - 32612216.
886	52.	Nurk S, Meleshko D, Korobeynikov A, Pevzner PA. metaSPAdes: a new versatile
887		metagenomic assembler. Genome Res. 2017;27(5):824-34; doi: 10.1101/gr.213959.116
888		PMID - 28298430.
889	53.	Bushnell B. BBTools Software Package. sourceforge.net/projects/bbmap/ Accessed.
890	54.	Uritskiy GV, DiRuggiero J, Taylor J. MetaWRAP-a flexible pipeline for genome-
891		resolved metagenomic data analysis. Microbiome. 2018;6(1):1-13; doi: 10.1186/s40168-
892		018-0541-1.
893	55.	Parks DH, Imelfort M, Skennerton CT, Hugenholtz P, Tyson GW. CheckM: assessing the
894		quality of microbial genomes recovered from isolates, single cells, and metagenomes.
895		Genome Res. 2015;25(7):1043-55.
896	56.	Chaumeil PA, Mussig AJ, hugenholtz p, Parks DH. GTDB-Tk: a toolkit to classify
897		genomes with the Genome Taxonomy Database. Bioinformatics. 2020;36(6):1925-7.
898	57.	Bowers RM, Kyrpides NC, Stepanauskas R, Harmon-Smith M, Doud D, Reddy TBK, et
899		al. Minimum information about a single amplified genome (MISAG) and a metagenome-
900		assembled genome (MIMAG) of bacteria and archaea. Nat Biotechnol. 2017;35(8):725-
901		31; doi: 10.1038/nbt.3893.
902	58.	Chen ECH, Morin E, Beaudet D, Noel J, Yildirir G, Ndikumana S, et al. High
903		intraspecific genome diversity in the model arbuscular mycorrhizal symbiont
904		Rhizophagus irregularis. New Phytol. 2018;220(4):1161-71; doi: 10.1111/nph.14989
905		PMID - 29355972.
906	59.	Wattam AR, Davis JJ, Assaf R, Boisvert S, Brettin T, Bun C, et al. Improvements to
907		PATRIC, the all-bacterial Bioinformatics Database and Analysis Resource Center.
908		Nucleic Acids Res. 2016;45(D1):D535-D42; doi: 10.1093/nar/gkw1017.

909	60.	Aramaki T, Blanc-Mathieu R, Endo H, Ohkubo K, Kanehisa M, Goto S, et al.
910		KofamKOALA: KEGG ortholog assignment based on profile HMM and adaptive score
911		threshold. Bioinformatics. 2019;36(7):2251-2; doi: 10.1093/bioinformatics/btz859 PMID
912		- 31742321.

- 913 61. Yin Y, Mao X, Yang J, Chen X, Mao F, Xu Y. dbCAN: a web resource for automated
 914 carbohydrate-active enzyme annotation. Nucleic Acids Res. 2012;40(W1):W445-W51;
 915 doi: 10.1093/nar/gks479.
- 82. Rawlings ND, Barrett AJ, Thomas PD, Huang X, Bateman A, Finn RD. The MEROPS
 83. database of proteolytic enzymes, their substrates and inhibitors in 2017 and a comparison
 84. with peptidases in the PANTHER database. Nucleic Acids Res. 2017;46(Database
 85. issue):gkx1134-; doi: 10.1093/nar/gkx1134 PMID 29145643.
- 920 63. Shimkets LJ. Myxobacteria, Development and Cell Interactions. Springer Ser Mol Biology. 1984:91-107; doi: 10.1007/978-1-4613-8280-5 4.
- 922 64. Parks DH, Chuvochina M, Rinke C, Mussig AJ, Chaumeil P-A, Hugenholtz P. GTDB: an
 923 ongoing census of bacterial and archaeal diversity through a phylogenetically consistent,
 924 rank normalized and complete genome-based taxonomy. Nucleic Acids Res.
 925 2021;50(D1):D785-D94; doi: 10.1093/nar/gkab776 PMID 34520557.
- Murphy CL, Yang R, Decker T, Cavalliere C, Andreev V, Bircher N, et al. Genomes of
 Novel Myxococcota Reveal Severely Curtailed Machineries for Predation and Cellular
 Differentiation. Appl Environ Microbiol. 2021;87(23):e01706-21; doi:
 10.1128/aem.01706-21 PMID 34524899.
- Mathieu S, Henrissat B, Labre F, Skjåk-Bræk G, Helbert W. Functional Exploration of
 the Polysaccharide Lyase Family PL6. PLoS ONE. 2016;11(7):e0159415; doi:
 10.1371/journal.pone.0159415 PMID 27438604.
- 67. Reji L, Cardarelli EL, Boye K, Bargar JR, Francis CA. Diverse ecophysiological
 adaptations of subsurface Thaumarchaeota in floodplain sediments revealed through
 genome-resolved metagenomics. ISME J. 2022;16(4):1140-52; doi: 10.1038/s41396-02101167-7 PMID 34873295.
- 93768.Gummadi SN, Panda T. Purification and biochemical properties of microbial938pectinases—a review. Process Biochem. 2003;38(7):987-96; doi: 10.1016/s0032-9399592(02)00203-0.
- 69. Elboutachfaiti R, Delattre C, Petit E, Michaud P. Polyglucuronic acids: Structures,
 functions and degrading enzymes. Carbohyd Polym. 2011;84(1):1-13; doi:
 10.1016/j.carbpol.2010.10.063.
- 943 70. Hestrin R, Hammer EC, Mueller CW, Lehmann J. Synergies between mycorrhizal fungi 944 and soil microbial communities increase plant nitrogen acquisition. Communications 945 Biology. 2019;2(1):1-9; doi: 10.1038/s42003-019-0481-8.
- P46 71. Emmett BD, Lévesque-Tremblay V, Harrison MJ. Conserved and reproducible bacterial
 p47 communities associate with extraradical hyphae of arbuscular mycorrhizal fungi. ISME J.
 p48 2021:1-13; doi: 10.1038/s41396-021-00920-2 PMID 33649552.
- 949 72. Morgan AD, MacLean RC, Hillesland KL, Velicer GJ. Comparative Analysis of
 950 Myxococcus Predation on Soil Bacteria. Appl Environ Microbiol. 2010;76(20):6920-7;
 951 doi: 10.1128/aem.00414-10 PMID 20802074.
- 952 73. Livingstone PG, Morphew RM, Whitworth DE. Myxobacteria Are Able to Prey Broadly
 953 upon Clinically-Relevant Pathogens, Exhibiting a Prey Range Which Cannot Be

954 Explained by Phylogeny. Front Microbiol. 2017;8:1593; doi: 10.3389/fmicb.2017.01593 955 PMID - 28878752. 956 Sutton D, Livingstone PG, Furness E, Swain MT, Whitworth DE. Genome-Wide 74. 957 Identification of Myxobacterial Predation Genes and Demonstration of Formaldehyde 958 Secretion as a Potentially Predation-Resistant Trait of Pseudomonas aeruginosa. Front 959 Microbiol. 2019;10:2650; doi: 10.3389/fmicb.2019.02650 PMID - 31798566. 960 Beier S, Bertilsson S. Bacterial chitin degradation-mechanisms and ecophysiological 75. 961 strategies. Front Microbiol. 2013;4:149; doi: 10.3389/fmicb.2013.00149 PMID -962 23785358. 963 76. Svitil AL, Chadhain S, Moore JA, Kirchman DL. Chitin Degradation Proteins Produced 964 by the Marine Bacterium Vibrio harveyi Growing on Different Forms of Chitin. Appl 965 Environ Microbiol. 1997;63(2):408-13; doi: 10.1128/aem.63.2.408-413.1997 PMID -966 16535505. 967 77. Li T, Li M, Hou L, Guo Y, Wang L, Sun G, et al. Identification and characterization of a 968 core fucosidase from the bacterium Elizabethkingia meningoseptica. J Biol Chem. 969 2018;293(4):1243-58; doi: 10.1074/jbc.m117.804252 PMID - 29196602. 970 78. Ihara H, Hanashima S, Tsukamoto H, Yamaguchi Y, Taniguchi N, Ikeda Y. 971 Difucosylation of chitooligosaccharides by eukaryote and prokaryote a1,6-972 fucosyltransferases. Biochimica Et Biophysica Acta Bba - Gen Subj. 973 2013;1830(10):4482-90; doi: 10.1016/j.bbagen.2013.05.013 PMID - 23688399. 974 79. Hooker JE, Piatti P, Cheshire MV, Watson CA. Polysaccharides and monosaccharides in 975 the hyphosphere of the arbuscular mycorrhizal fungi Glomus E3 and Glomus tenue. Soil 976 Biol Biochem. 2007;39(2):680-3; doi: 10.1016/j.soilbio.2006.08.006. 977 80. Rush TA, Puech-Pagès V, Bascaules A, Jargeat P, Maillet F, Haouy A, et al. Lipo-978 chitooligosaccharides as regulatory signals of fungal growth and development. Nat 979 Commun. 2020;11(1):3897; doi: 10.1038/s41467-020-17615-5 PMID - 32753587. 980 81. Maillet F, Poinsot V, André O, Puech-Pagès V, Haouy A, Gueunier M, et al. Fungal 981 lipochitooligosaccharide symbiotic signals in arbuscular mycorrhiza. Nature. 982 2011;469(7328):58-63; doi: 10.1038/nature09622 PMID - 21209659. 983 82. Rehm BHA, Valla S. Bacterial alginates: biosynthesis and applications. Appl Microbiol 984 Biotechnol. 1997;48(3):281-8; doi: 10.1007/s002530051051 PMID - 9352672. 985 83. Peterson BJ, Fry B. Stable Isotopes in Ecosystem Studies. Annu Rev Ecol Syst. 986 1987;18(1):293-320; doi: 10.1146/annurev.es.18.110187.001453. 987 Nicol GW, Leininger S, Schleper C, Prosser JI. The influence of soil pH on the diversity, 84. 988 abundance and transcriptional activity of ammonia oxidizing archaea and bacteria. 989 Environ Microbiol. 2008;10(11):2966-78; doi: 10.1111/j.1462-2920.2008.01701.x. 990 Zhang L-M, Offre PR, He J-Z, Verhamme DT, Nicol GW, Prosser JI. Autotrophic 85. 991 ammonia oxidation by soil thaumarchaea. Proc Natl Acad Sci USA. 2010;107(40):17240-992 5; doi: 10.1073/pnas.1004947107 PMID - 20855593. 993 Tourna M, Stieglmeier M, Spang A, Könneke M, Schintlmeister A, Urich T, et al. 86. 994 Nitrososphaera viennensis, an ammonia oxidizing archaeon from soil. Proc Natl Acad Sci 995 USA. 2011;108(20):8420-5; doi: 10.1073/pnas.1013488108 PMID - 21525411. 996 87. Chen Y-L, Chen B-D, Hu Y-J, Li T, Zhang X, Hao Z-P, et al. Direct and indirect 997 influence of arbuscular mycorrhizal fungi on abundance and community structure of 998 ammonia oxidizing bacteria and archaea in soil microcosms. Pedobiologia. 2013;56(4-999 6):205-12; doi: 10.1016/j.pedobi.2013.07.003.

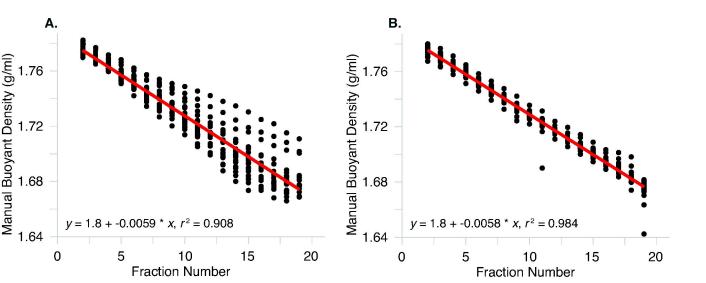
Bukovská P, Bonkowski M, Konvalinková T, Beskid O, Hujslová M, Püschel D, et al.

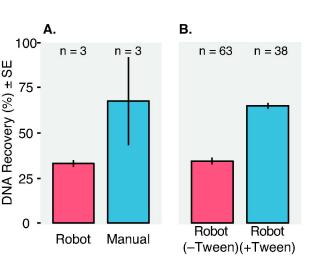
1000

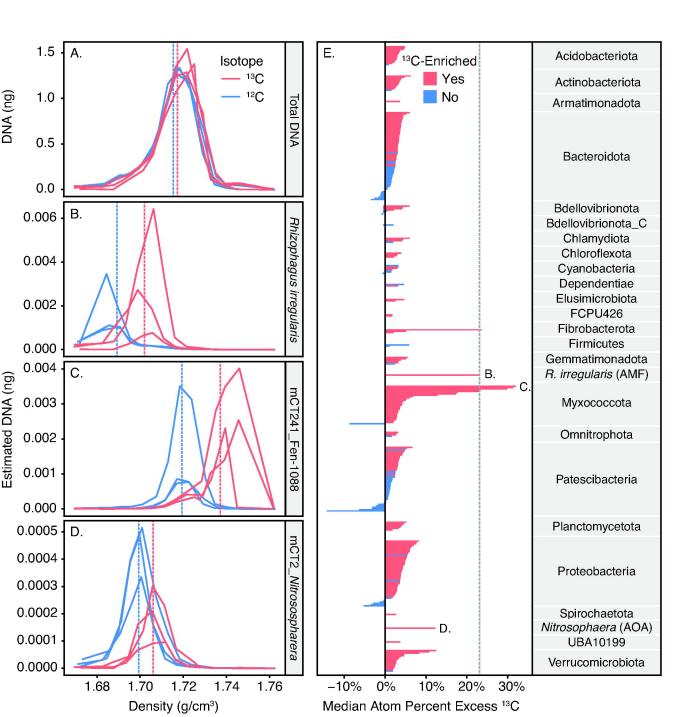
88.

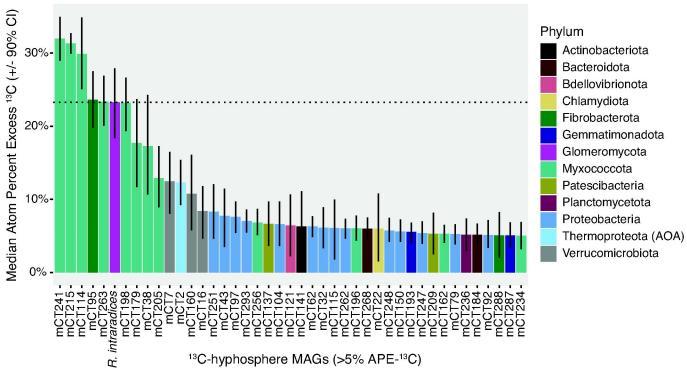
1001 Utilization of organic nitrogen by arbuscular mycorrhizal fungi-is there a specific role 1002 for protists and ammonia oxidizers? Mycorrhiza. 2018;28(3):269-83; doi: 1003 10.1007/s00572-018-0825-0 PMID - 29455336. 1004 89. Bukovská P, Gryndler M, Gryndlerová H, Püschel D, Jansa J. Organic Nitrogen-Driven 1005 Stimulation of Arbuscular Mycorrhizal Fungal Hyphae Correlates with Abundance of 1006 Ammonia Oxidizers. Front Microbiol. 2016;7(149):859; doi: 10.3389/fmicb.2016.00711. 1007 90. Wattenburger CJ, Gutknecht J, Zhang Q, Brutnell T, Hofmockel K, Halverson L. The 1008 rhizosphere and cropping system, but not arbuscular mycorrhizae, affect ammonia 1009 oxidizing archaea and bacteria abundances in two agricultural soils. Appl Soil Ecol. 2020;151:103540; doi: 10.1016/j.apsoil.2020.103540. 1010 1011 91. Kozlowski JA, Stieglmeier M, Schleper C, Klotz MG, Stein LY. Pathways and key 1012 intermediates required for obligate aerobic ammonia-dependent chemolithotrophy in 1013 bacteria and Thaumarchaeota. ISME J. 2016;10(8):1836-45; doi: 10.1038/ismej.2016.2 1014 PMID - 26882267. 1015 92. Staddon PL, Ramsey CB, Ostle N, Ineson P, Fitter AH. Rapid turnover of hyphae of 1016 mycorrhizal fungi determined by AMS microanalysis of C-14. Science. 1017 2003;300(5622):1138-40. 1018 93. See CR, Keller AB, Hobbie SE, Kennedy PG, Weber PK, Pett-Ridge J. Hyphae move 1019 matter and microbes to mineral microsites: Integrating the hyphosphere into conceptual 1020 models of soil organic matter stabilization. Global Change Biol. 2022;28(8):2527-40; doi: 1021 10.1111/gcb.16073 PMID - 34989058. 1022 94. Wright SF, Franke-Snyder M, Morton JB, Upadhyaya A. Time-course study and partial 1023 characterization of a protein on hyphae of arbuscular mycorrhizal fungi during active 1024 colonization of roots. Plant Soil. 1996;181(2):193-203; doi: 10.1007/bf00012053. 1025 95. Montgomery L, Flesher B, Stahl D. Transfer of Bacteroides succinogenes (Hungate) to 1026 Fibrobacter gen. nov. as Fibrobacter succinogenes comb. nov. and description of 1027 Fibrobacter intestinalis sp. nov. Int J Syst Bacteriol. 1988;38(4):430-5; doi: 1028 10.1099/00207713-38-4-430. 1029 96. Ivanova AA, Wegner CE, Kim Y, Liesack W, Dedysh SN. Identification of microbial 1030 populations driving biopolymer degradation in acidic peatlands by metatranscriptomic 1031 analysis. Mol Ecol. 2016;25(19):4818-35; doi: 10.1111/mec.13806. 1032 97. Rahman NA, Parks DH, Vanwonterghem I, Morrison M, Tyson GW, Hugenholtz P. A 1033 phylogenomic analysis of the bacterial phylum Fibrobacteres. Front Microbiol. 1034 2016;6(149):1469; doi: 10.3389/fmicb.2015.01469. 1035 98. Edwards J, Johnson C, Santos-Medellín C, Lurie E, Podishetty NK, Bhatnagar S, et al. 1036 Structure, variation, and assembly of the root-associated microbiomes of rice. Proc Natl 1037 Acad Sci USA. 2015;112(8):E911-E20; doi: 10.1073/pnas.1414592112. 1038 99. van Passel MWJ, Kant R, Palva A, Copeland A, Lucas S, Lapidus A, et al. Genome 1039 sequence of the Verrucomicrobium Opitutus terrae PB90-1, an abundant inhabitant of 1040 rice paddy soil ecosystems. J Bacteriol. 2011;193(9):2367-8; doi: 10.1128/JB.00228-11. 100. Wertz JT, Kim E, Breznak JA, Schmidt TM, Rodrigues JLM. Genomic and physiological

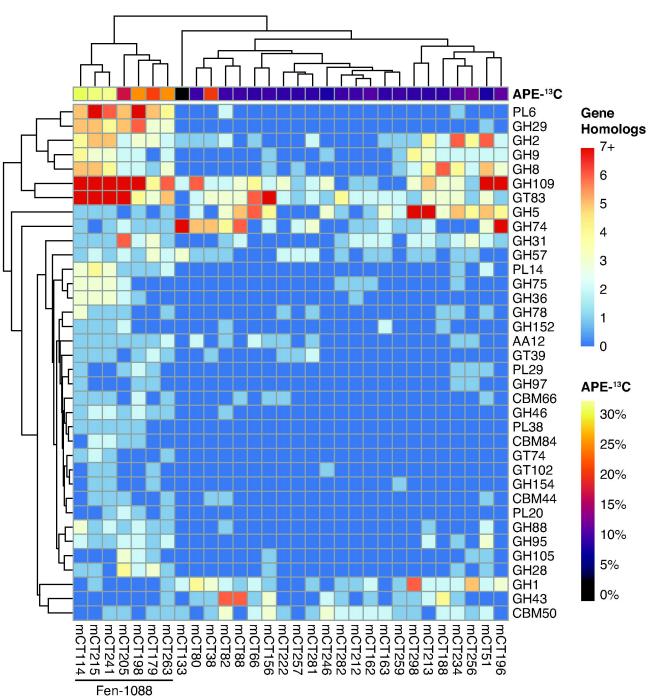
1041 100. Wertz JT, Kim E, Breznak JA, Schmidt TM, Rodrigues JLM. Genomic and physiological 1042 characterization of the Verrucomicrobia isolate *Diplosphaera colitermitum* gen. nov., sp. 1043 nov., reveals microaerophily and nitrogen fixation genes. Appl Environ Microbiol. 1044 2012;78(5):1544-55; doi: 10.1128/AEM.06466-11. 1045 101. Lin JY, Russell JA, Sanders JG, Wertz JT. Cephaloticoccus gen. nov., a new genus of 1046 'Verrucomicrobia' containing two novel species isolated from Cephalotes ant guts. Int J 1047 Syst Evol Microbiol. 2016;66(8):3034-40; doi: 10.1099/ijsem.0.001141. 1048 102. Hünninghaus M, Dibbern D, Kramer S, Koller R, Pausch J, Schloter-Hai B, et al. 1049 Disentangling carbon flow across microbial kingdoms in the rhizosphere of maize. Soil 1050 Biol Biochem. 2019;134:122-30; doi: 10.1016/j.soilbio.2019.03.007. 1051 Nuccio EE, Starr E, Karaoz U, Brodie EL, Zhou J, Tringe SG, et al. Niche differentiation 103. 1052 is spatially and temporally regulated in the rhizosphere. ISME J. 2020;269(9):1-16; doi: 1053 10.1038/s41396-019-0582-x. 1054 104. Kersten W, Kersten H, Szybalski W, Fiandt M. Physicochemical Properties of 1055 Complexes between Deoxyribonucleic Acid and Antibiotics Which Affect Ribonucleic 1056 Acid Synthesis (Actinomycin, Daunomycin, Cinerubin, Nogalamycin, Chromomycin, 1057 Mithramycin, and Olivomycin) *. Biochemistry. 1966;5(1):236-44; doi: 1058 10.1021/bi00865a031 PMID - 4161040. 1059











Myxococcota MAGs